www.czasopisma.pan.pl PAN POLSKA AKADEMIA NAUK www.journals.pan.pl

PAN ARCHIVES OF ACOUSTICS
Vol. **45**, No. 1, pp. 49–66 (2020)
DOI: 10.24425/aoa.2020.132481



Research Paper

# Investigation on the Effects of Acoustic Liner Variation and Geometry Discontinuities on the Acoustic Performance of Lined Ducts

Raja DHIEF[(1),(2)], Amine MAKNI[(2)], Mohamed TAKTAK[(1),(2)*]
Mabrouk CHAABANE[(1)], Mohamed HADDAR[(2)]

[(1)] *Faculty of Sciences of Sfax*
BP 1171, 3000 Sfax, Tunisia
*Corresponding Author e-mail: mohamed.taktak@fss.rnu.tn

[(2)] *Laboratory of Mechanics, Modeling and Production (LA2MP)*
*National School of Engineers of Sfax, University of Sfax*
Sfax, Tunisia

(*received April 23, 2019; accepted November 4, 2019*)

Noise reduction inside waveguide systems has gained momentum owing to a great interest in it. To attenuate the sound in a broad frequency range, this study aims to compare the effects of two acoustic liners, a perforated plate backed by an air cavity (PP-Air cavity), or by a porous material (PP-PM), on the acoustic behaviour of lined ducts using a numerical model to compute the multimodal scattering matrix. From this matrix, the reflection and the transmission coefficients are computed and therefore the acoustic power attenuation is deduced. Moreover, the effects of geometry of ducts with and without changes in the section are investigated. The numerical results are obtained for five configurations, including cases of narrowing and widening of a duct portion with sudden or progressive discontinuities. Accordingly, numerical coefficients of reflection and transmission as well as the acoustic power attenuation show the relative influence of acoustic liners in each type of configuration.

**Keywords:** absorbent systems effect; discontinuities effect; scattering matrix; acoustic power attenuation.

## 1. Introduction

Noise reduction in waveguide systems is a topic of considerable interest with respect to several applications, such as aircraft engines, compressors, and building ventilation systems. These systems encompass numerous geometric forms as duct systems, which has an important role in the studies of the behaviour of sound waves. The acoustic propagation has been investigated, first in rigid cylindrical, see (Auger, Ville, 1986), and rectangular ducts, see (Muehleisen, 1996). Besides, acoustics liners are used as a treatment of duct walls. These liners consist of materials that are able to reduce the transmission of sound along the ducts and provide a good attenuation at medium and high frequencies. Several methods were developed to extract the acoustic impedance, the related acoustic liner properties, under grazing flow conditions such as those presented by Jones and Watson (2011; 2013), Jones *et al.* (2013), Busse-Gerstengarbe *et al.* (2012; 2013). Some methods, afterwards, were improved to incorporate the effect of high temperatures, as proposed by Kabral *et al.* (2014), Bodén and Kabral (2015). These works were carried out with respect to ducts without section change. Some waveguides can contain many variations in cross-sections, called discontinuities, which produce internal reflections of sound waves. The discontinuity problem in ducts was firstly investigated by Miles (1946). He showed that the sudden discontinuity in a cylindrical duct is analogous to lumped impedance. The transmission of sound in the case where the walls of the duct with sudden area expansion and extended inlet, treated by acoustically absorbing materials of finite length, is investigated by Demir (2016). In another work Demir (2017) defined the scattering matrices with the help of the Wiener-Hop technique in a non-uniformly lined duct with an inserted expansion chamber. Measurement of acoustic transmission matrix and acoustic power dissipation of duct discontinuity was described in (Sitel *et al.*,

2003). The analysis of discontinuities in rectangular ducts and higher order mode excitations using transmission line matrix (TLM) method and finite element method (FEM) is studied in (Masri, 2004).

The scattering matrix method has been widely used to characterise ducts with geometric discontinuities and ruptures wall impedance. This matrix provides a characterisation of lined duct, independently of the upstream and downstream conditions. The scattering matrix coefficients give an insight into transmission and reflection in a multimodal context. This latter can describe the energetic state of the duct element. The scattering matrix has been obtained in some previous works, using experimental approaches such as (Ville, 2014; Taktak *et al.*, 2008). Some other works dealt with calculation of the scattering matrix through numerical methods. The finite element method was indeed used to model a 3D axisymmetric duct, see (Taktak *et al.*, 2010). Therefore, this matrix was used to evaluate the effect of temperature on the acoustic behaviour of the duct element lined with porous materials (Ben Jdidia *et al.*, 2014). Besides, the effect of liner characteristics composed of a perforated plate and absorbing porous material backed by a rigid plate on the acoustic performance of a duct element was investigated in (Othmani *et al.*, (2015). Some works used experimental methods to describe the duct discontinuity for higher order acoustic duct mode propagation, such as (Sitel, Ville, 2006) that developed a procedure for measuring the scattering matrix of straight and reactive type silencer duct configurations. The effect of duct diameter increase and duct diameter decrease on the acoustic behaviour of the wall or lined duct was examined numerically by Masmoudi *et al.*, 2017. The numerical method was developed to incorporate the flow effect in (Taktak *et al.*, 2012; 2013). To compute the propagation in the case of 2D lined duct with the flow, Aurégan *et al.* (2004) proposed to couple an analytical model and measurements scattering matrix in the hard wall ducts.

In this paper we extend our previous work (Taktak *et al.* 2010) to study the effect of geometry of ducts treated by acoustic liners. Therefore, a comparison between acoustic liners' effects on the acoustic performance of different lined ducts' configurations is presented. This investigation is based on the computation of the reflection, transmission, and the acoustic power attenuation for each configuration, through the calculation of the scattering matrix. This aim is achieved by studying two types of liners: a perforated plate backed by an air cavity, or by a porous material. The numerical results are obtained for various configurations, including cases of narrowing and widening of a portion duct with sudden or progressive discontinuities. The paper is structured as follows: in Sec. 2, the numerical computation of the multimodal scattering matrix is presented. Section 3 displays the acoustic power attenuation computation. Section 4 evinces the models of locally reacting impedance for the studied liners. Finally, the numerical results are presented and discussed in Sec. 5.

## 2. Configurations of the studied ducts

Geometry of the studied ducts is depicted in Fig. 1. A shape of each duct under consideration is a rigid-lined-rigid cylindrical duct located between two axial coordinates $Z_R$ and $Z_L$.

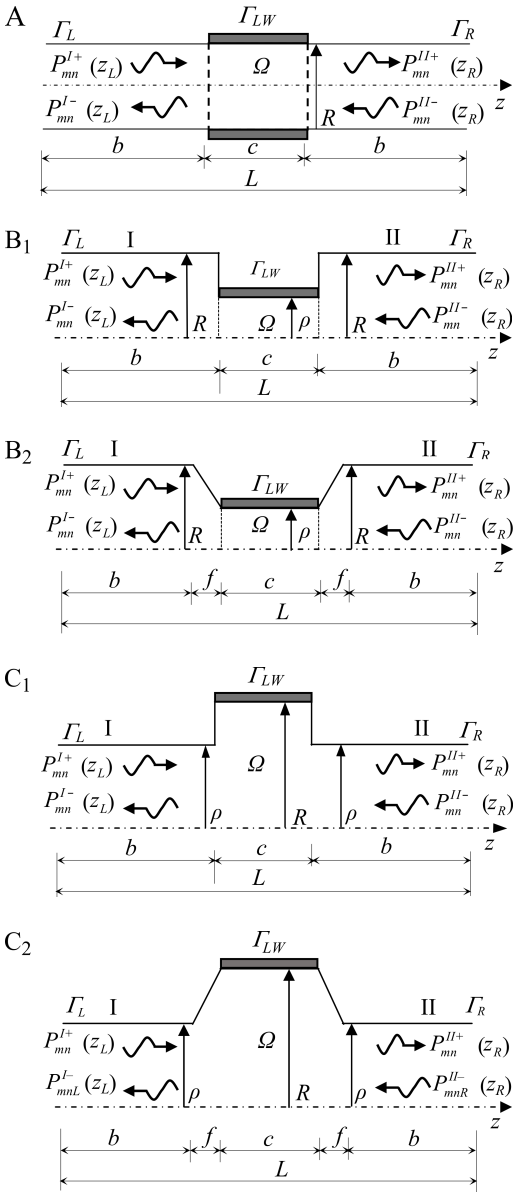


Fig. 1. Geometry of the ducts: A – straight duct; B – symmetric part of ducts, having a narrowing of a portion with two types of discontinuities under consideration: $f = 0$, sudden discontinuity, and $f \neq 0$, progressive discontinuity; C – symmetric part of ducts, having a widening of a portion with two types of discontinuities under consideration: $f = 0$, sudden discontinuity, and $f \neq 0$, progressive discontinuity.

The scattering matrix is computed in each duct element of length $L = 1$ m and radius changing depending on the configuration type. The radius $a = R = 0.075$ m for the first configuration A (wherein a constant circular section) and for the geometry $B_1$ and $B_2$ of a sudden and progressive narrowing in a portion of duct element. The radius $a = \rho = 0.055$ m for the geometry C of a sudden or progressive widening in a portion of the duct element. The duct diameter increases in the case of widening of the portion duct, and the duct diameter decreases in the case when the narrowing of a portion duct is 0.02 m. The edge of the studied ducts is composed of four parts: the rigid wall duct part $\Gamma_{WD}$, the lined duct part $\Gamma_{LD}$, the left transversal boundary $\Gamma_L$, and the right transversal boundary $\Gamma_R$ are characterised, respectively, by their normal vectors $\mathbf{n}$. In the lined part of the duct, the liner is modelled by two acoustic impedances $Z_a$ and $Z_b$.

## 3. Computation of the multimodal scattering matrix

### 3.1. Definition of the scattering matrix

The multimodal scattering matrix $\mathbf{S}_{2N\times 2N}$ of the element duct relates the outcoming pressure waves array $\mathbf{P}_{2N}^{\text{out}} = \left\langle P_{00}^{I-}, ..., P_{PQ}^{I-}, P_{00}^{II+}, ..., P_{PQ}^{II+} \right\rangle_N^T$ to the incoming pressure waves array $\mathbf{P}_{2N}^{\text{in}} = \left\langle P_{00}^{I+}, ..., P_{PQ}^{I+}, P_{00}^{II-}, ..., P_{PQ}^{II-} \right\rangle_N^T$ (Fig. 1) (Abom, 1991; Taktak *et al.*, 2010) as follows:

$$\mathbf{P}_{2N}^{\text{out}} = \mathbf{S}_{2N\times 2N}\mathbf{P}_{2N}^{\text{in}} = \begin{bmatrix} \mathbf{R}_{N\times N}^{I} & \mathbf{T}_{N\times N}^{I} \\ \mathbf{T}_{N\times N}^{II} & \mathbf{R}_{N\times N}^{II} \end{bmatrix}_{2N\times 2N} \mathbf{P}_{2N}^{\text{in}}, \quad (1)$$

where $\left(P_{mn}^{I+}, P_{mn}^{I-}\right)$ and $\left(P_{mn}^{II+}, P_{mn}^{II-}\right)$ are the modal pressure coefficients associated with the $(m, n)$ mode travelling, respectively, in the positive and negative directions in the region $I$ and $II$. $m$ and $n$ are, respectively, the azimuthal and the radial mode numbers, $N$ is the number of modes in both cross sections, $P$ and $Q$ are, respectively, the angular and radial wave numbers associated with the $N$-th propagating mode ($m \le P$ and $n \le Q$).

The boundary effects at the inlet and outlet of the duct are neglected. The acoustic pressure $p$ in each cylindrical duct is the solution of the system, containing the Helmholtz equation with boundaries conditions, respectively, at $\Gamma_{WD}$ (rigid wall duct part) and $\Gamma_{LD}$ (lined duct part), as presented in a previous work (Taktak *et al.*, 2010):

$$\begin{cases} \Delta p + k^2 p = 0 & (\Omega), \\ Z\dfrac{\partial p}{\partial n_{LD}} = i\omega\rho_0 p & (\Gamma_{LD}), \\ \dfrac{\partial p}{\partial n_{WD}} = 0 & (\Gamma_{WD}), \end{cases} \quad (2)$$

where $k$ is the total wave number, $\rho_0$ is the density of the air conditioning and $\omega$ is the pulsation. The acoustic pressure fields at the left section $\Gamma_L$ and the right section $\Gamma_R$ (Fig. 1) are given as follows:

$$\begin{aligned} P^L &= \sum_{n=1}^{Nr} n_L \left( P_{mn}^{I+} e^{ik_{mn}(z-z_L)} + P_{mn}^{I-} e^{ik_{mn}(z-z_L)} \right) J_m\left(\frac{\chi_{mn}}{a} r\right), \\ P^R &= \sum_{n=1}^{Nr} n_R \left( P_{mn}^{II+} e^{ik_{mn}(z-z_R)} + P_{mn}^{II-} e^{ik_{mn}(z-z_R)} \right) J_m\left(\frac{\chi_{mn}}{a} r\right). \end{aligned} \quad (3)$$

$N_r$ is the number of radial modes, $J_m$ is the Bessel function of the first kind of order $m$, $r$ is the radial variable, and $\chi_{mn}$ is the $n$-th root satisfying the radial hard-boundary condition on the rigid-wall of the main duct, $k_{mn}$ are the axial wave numbers associated with the $(m, n)$ mode and defined as:

$$k_{mn} = \pm\sqrt{k^2 - k_t^2}, \quad (4)$$

$k_t$ is the transverse wave number.

### 3.2. Variational formulation

To solve the system of Eqs (2), the finite element method is used. The corresponding weak variational formulation is written as follows:

$$\begin{aligned} \Pi = &\int_\Omega -(\nabla q \cdot \nabla p) r \,\mathrm{d}r\,\mathrm{d}z \\ &+ \frac{1}{c^2}\int_\Omega ((i\omega q)(-i\omega p)) r \,\mathrm{d}r\,\mathrm{d}z \\ &- \rho_0\omega^2 \int_{\Gamma_{LD}} q\frac{p}{i\omega Z} r \,\mathrm{d}\Gamma_{LD} \\ &+ \sum_{n=1}^{Nr} i n_L \left\{ k_{mn} P_{mn}^{I+} + k_{mn} P_{mn}^{I-} \right\} \\ &\times \int_{\Gamma_L} q J_m\left(\frac{\chi_{mn}}{a} r\right) r \,\mathrm{d}\Gamma_L \\ &+ \sum_{n=1}^{Nr} i n_R \left\{ k_{mn} P_{mn}^{II+} + k_{mn} P_{mn}^{II-} \right\} \\ &\times \int_{\Gamma_R} q J_m\left(\frac{\chi_{mn}}{a} r\right) r \,\mathrm{d}\Gamma_R = 0, \end{aligned} \quad (5)$$

where $p$ and $q$ are the acoustic pressure in the duct and the test function, respectively.

The use of modal decomposition at the boundaries $\Gamma_L$ and $\Gamma_R$ in Eq. (3) introduces the modal pressures as additional degrees of freedom of the model. It is necessary to obtain a well posed problem. This is conducted by supposing that pressures at $\Gamma_L$ and $\Gamma_R$ are

obtained by the projection of the acoustic field over the eigenfunctions of the rigid wall duct:

$$\begin{aligned}\int_{\Gamma_L} pJ_m\left(\frac{\chi_{mn}}{a}r\right)\mathrm{d}\Gamma_L &= a^*,\\ \int_{\Gamma_R} pJ_m\left(\frac{\chi_{mn}}{a}r\right)\mathrm{d}\Gamma_R &= b^*,\end{aligned} \tag{6}$$

where

$$a^* = \left(P^{I+}_{mn} + P^{I-}_{mn}\right)\int_{\Gamma_L} J_m\left(\frac{\chi_{mn}}{a}r\right)^2 r\,\mathrm{d}\Gamma_L,$$

$$b^* = \left(P^{II+}_{mn} + P^{II-}_{mn}\right)\int_{\Gamma_R} J_m\left(\frac{\chi_{mn}}{a}r\right)^2 r\,\mathrm{d}\Gamma_R.$$

### 3.3. Finite element discretisation

To solve the proposed problem, the domain ($\Omega$) is discretised with triangular finite elements, while edges are meshed by two node finite elements. The computation of integrals of Eq. (5) is made by summation over the finite elements number of elementary integrals, as presented by Dhatt and Touzot (1989):

$$\begin{aligned}I_e = &\underbrace{\int_{\Omega_e} -(\nabla q\cdot\nabla p)r\,\mathrm{d}r_e\,\mathrm{d}z_e + \frac{1}{c^2}\int_{\Omega_e}(i\omega q)(-i\omega p)r\,\mathrm{d}r_e\,\mathrm{d}z_e}_{I_{e1}}\\ &\underbrace{+ -\rho_0\omega^2\int_{\Gamma_e} q\frac{p}{i\omega Z}r\,\mathrm{d}\Gamma_e}_{I_{e2}}\\ &\underbrace{+\sum_{n=1}^{Nr} in_L\left[k_{mn}P^{I+}_{mn} + k_{mn}P^{I-}_{mn}\right]\int_{\Gamma_e} qJ_m\left(\tfrac{\chi_{mn}}{a}r\right)r\,\mathrm{d}\Gamma_e}_{I_{e3}}\\ &\underbrace{+\sum_{n=1}^{Nr} in_R\left[k_{mn}P^{II+}_{mn} + k_{mn}P^{II-}_{mn}\right]\int_{\Gamma_e} qJ_m\left(\tfrac{\chi_{mn}}{a}r\right)r\,\mathrm{d}\Gamma_e}_{I_{e4}}.\end{aligned} \tag{7}$$

The computation of integrals (7) is obtained by summation over the finite elements number of elementary integrals

$$\begin{aligned}I_{e5} = &\int_{\Gamma_e} pJ_m\left(\frac{\chi_{mn}}{a}r\right)r\,\mathrm{d}\Gamma_e\\ &-\left(P^{I+}_{mn} + P^{I-}_{mn}\right)\int_{\Gamma_e} J_m\left(\frac{\chi_{mn}}{a}r\right)^2 r\,\mathrm{d}\Gamma_e,\\ I_{e6} = &\int_{\Gamma_e} pJ_m\left(\frac{\chi_{mn}}{a}r\right)r\,\mathrm{d}\Gamma_e\\ &-\left(P^{II+}_{mn} + P^{II-}_{mn}\right)\int_{\Gamma_e} J_m\left(\frac{\chi_{mn}}{a}r\right)^2 r\,\mathrm{d}\Gamma_e,\end{aligned} \tag{8}$$

where $\mathrm{d}r_e\,\mathrm{d}z_e$ and $\Gamma_e$ are, respectively, the elementary triangular and two-node finite elements.

#### 3.3.1. Elementary computation of the triangular finite element

For the triangular finite element composed of three nodes, the integral $I_{e1}$ is written as follows:

$$\begin{aligned}I_{e1} &= \langle q_1\,q_2\,q_3\rangle\,\mathbf{K}_{e1}\,\langle q_1\,q_2\,q_3\rangle^T,\\ (\mathbf{K}_e)_1 &= \int_{\Omega_{ref}} -\left(\nabla q\cdot\nabla p^T\right)\det\mathbf{j}r\,\mathrm{d}\xi\,\mathrm{d}\eta\\ &+\int_{\Omega_{ref}}\left(\frac{i\omega}{c}\begin{Bmatrix}N_1'\\ N_2'\\ N_3'\end{Bmatrix}\left(-\frac{i\omega}{c}\left[N_1',\ N_2',\ N_3'\right]\right)\right)\det\mathbf{j}r\,\mathrm{d}\xi\,\mathrm{d}\eta,\end{aligned} \tag{9}$$

where $p_i = 1,2,3$ and $q_i = 1,2,3$ are, respectively, nodal acoustic pressures and nodal test functions of the triangular finite element, $\mathbf{j}$ is the inverse matrix of the Jacobian matrix $\mathbf{J}$ of the transformation from the reference element to the real base and $N_1'(\xi,\eta)$, $N_2'(\xi,\eta)$ and $N_3'(\xi,\eta)$ are the interpolation functions of the triangular element, as presented by Dhatt and Touzot (1989)

$$\begin{aligned}N_1'(\xi,\eta) &= 1-\xi-\eta, \qquad N_2'(\xi,\eta) = \xi,\\ N_3'(\xi,\eta) &= \eta.\end{aligned} \tag{10}$$

The integration of the integral (9) is made by using the numerical Gauss integration method, see Dhatt and Touzot (1989). Finally, the global corresponding matrix is:

$$\mathbf{K}_1 = \sum_{1}^{Nelt}(\mathbf{K}_e)_1, \tag{11}$$

here *Nelt* is the number of triangular finite elements.

#### 3.3.2. Elementary computations of the two nodes finite element

For the two-node finite element belonging to the lined part of the duct composed of two nodes, $I_{e2}$ and $I_{e3}$ are computed as follows:

$$I_{e2} = [q_1,\,q_2]\,(\mathrm{K}_e)_2\begin{Bmatrix}p_1\\ p_2\end{Bmatrix},$$

$$\begin{aligned}(\mathbf{K}_e)_2 = &\rho_0 i\omega\int_{-1}^{1}\begin{Bmatrix}N_1\\ N_2\end{Bmatrix}[N_1,\,N_2]\\ &\cdot\frac{[N_1,\,N_2]}{\left([Z_{n1},\,Z_{n2}]\begin{Bmatrix}N_1\\ N_2\end{Bmatrix}\right)}\frac{L_e}{2}r\,\mathrm{d}\xi,\end{aligned} \tag{12}$$

where $p_i = 1,2$ and $q_i = 1,2$ are nodal acoustic pressures and nodal test functions of the two-node finite element, respectively. $Z_{n1}$ and $Z_{n2}$ are the acoustic impedance of each node of the two-node finite element, $L_e$ is the

finite element length, $N_1(\xi)$ and $N_2(\xi)$ are the interpolation functions of the two-node finite element defined in (Dhatt, Touzot, 1989) as follows:

$$N_1(\xi,\eta) = \frac{1-\xi}{2}, \qquad N_2(\xi,\eta) = \frac{1+\xi}{2}. \tag{13}$$

The computation of $I_{e3}$ is written as follows for a finite element belonging to the left boundary:

$$I_{e3} = [q_1, q_2](\mathbf{K}_e)_3^+ \left(P_{mn}^{I+}\right)_{Nr} + [q_1, q_2](\mathbf{K}_e)_3^- \left(P_{mn}^{I-}\right)_{Nr},$$

$$(\mathbf{K}_e)_3^{\pm} = \begin{bmatrix} \dots & -ik_{mn}\int_{-1}^{1} N_1(\xi)\, J_m\left(\frac{\chi_{mn}}{a}r\right)\frac{L_e}{2}r\,\mathrm{d}\xi & \dots \\ \cdots & -ik_{mn}\int_{-1}^{1} N_2(\xi)\, J_m\left(\frac{\chi_{mn}}{a}r\right)\frac{L_e}{2}r\,\mathrm{d}\xi & \cdots \end{bmatrix}_{2Nr}. \tag{14}$$

The integral $I_{e4}$ for a two-node finite element belonging to the right boundary is written as follows:

$$I_{e4} = [q_1, q_2](\mathbf{K}_e)_4^+ \left(P_{mn}^{II+}\right)_{Nr} + [q_1, q_2](\mathbf{K}_e)_4^- \left(P_{mn}^{II-}\right)_{Nr},$$

$$(\mathbf{K}_e)_4^{\pm} = \begin{bmatrix} \dots & +ik_{mn}\int_{-1}^{1} N_1(\xi)\, J_m\left(\frac{\chi_{mn}}{a}r\right)\frac{L_e}{2}r\,\mathrm{d}\xi & \dots \\ \cdots & +ik_{mn}\int_{-1}^{1} N_2(\xi)\, J_m\left(\frac{\chi_{mn}}{a}r\right)\frac{L_e}{2}r\,\mathrm{d}\xi & \cdots \end{bmatrix}_{2Nr}. \tag{15}$$

The integrals $I_{e5}$ and $I_{e6}$ are obtained by means of linear interpolation of the pressure as follows:

$$I_{e5} = (\mathbf{K}_e)_{51}\begin{Bmatrix} P_1 \\ P_2 \end{Bmatrix} + (\mathbf{K}_e)_{52}^+ \left(\mathbf{P}_{mn}^{I+}\right)_{Nr} + (\mathbf{K}_e)_{52}^- \left(\mathbf{P}_{mn}^{I-}\right)_{Nr},$$

$$I_{e6} = (\mathbf{K}_e)_{61}\begin{Bmatrix} P_1 \\ P_2 \end{Bmatrix} + (\mathbf{K}_e)_{62}^+ \left(\mathbf{P}_{mn}^{II+}\right)_{Nr} + (\mathbf{K}_e)_{62}^- \left(\mathbf{P}_{mn}^{II-}\right)_{Nr},$$

$$(\mathbf{K}_e)_{51} = (\mathbf{K}_e)_{61} = \begin{bmatrix} \vdots & \vdots \\ \int_{-1}^{1} N_1(\xi)\, J_m\left(\frac{\chi_{mn}}{a}r\right)\frac{L_e}{2}r\,\mathrm{d}\xi & \int_{-1}^{1} N_2(\xi)\, J_m\left(\frac{\chi_{mn}}{a}r\right)\frac{L_e}{2}r\,\mathrm{d}\xi \\ \vdots & \vdots \end{bmatrix}_{2Nr},$$

$$(\mathbf{K}_e)_{52}^+ = (\mathbf{K}_e)_{52}^- = (\mathbf{K}_e)_{62}^+ = (\mathbf{K}_e)_{62}^- = \left[\mathrm{diag}\left(\int_{-1}^{1} J_m\left(\frac{\chi_{mn}}{a}r\right)^2 \frac{L_e}{2}r\,\mathrm{d}\xi\right)\right]_{Nr\times Nr}. \tag{16}$$

Once the elementary integrals are computed, the assembly of them is obtained as follows:

$$\mathbf{K}_3^{\pm} = \sum_{1}^{NelL} (\mathbf{K}e)_3^{\pm}, \qquad \mathbf{K}_4^{\pm} = \sum_{1}^{NelR} (\mathbf{K}e)_4^{\pm}, \tag{17}$$

where $N_{elL}$ and $N_{elR}$ are, respectively, the numbers of two-node elements at the left and right boundaries, and presented as follows:

$$\mathbf{K}_{51} = \sum_{1}^{NelL} (\mathbf{K}_e)_{51}, \qquad \mathbf{K}_{52}^{\pm} = \sum_{1}^{NelL} \left(\mathbf{K}_e^{\pm}\right)_{52},$$
$$\mathbf{K}_{61} = \sum_{1}^{NelR} (\mathbf{K}_e)_{61}, \qquad \mathbf{K}_{62}^{\pm} = \sum_{1}^{NelR} \left(\mathbf{K}_e^{\pm}\right)_{62}. \tag{18}$$

The arrangement of the previous system leads to the following matrix system:

$$\begin{bmatrix} \mathbf{K}_{M\times M} & a^* & a^{**} & b^* & b^{**} \\ c^* & c^{**} & c^{***} & 0 & 0 \\ 0 & 0 & 0 & 0 & 0 \\ 0 & 0 & 0 & 0 & 0 \\ d^* & 0 & 0 & d^{**} & d^{***} \end{bmatrix} \begin{Bmatrix} \begin{Bmatrix} p_1 \\ \vdots \\ p_M \end{Bmatrix}_M \\ \left\{\mathbf{P}_{mn}^{I-}\right\}_{Nr} \\ \left\{\mathbf{P}_{mn}^{I+}\right\}_{Nr} \\ \left\{\mathbf{P}_{mn}^{II-}\right\}_{Nr} \\ \left\{\mathbf{P}_{mn}^{II+}\right\}_{Nr} \end{Bmatrix} = 0, \tag{19}$$

$$\mathbf{K}_{M\times M} = \mathbf{K}_1,$$

where

$$a^* = \left(\mathbf{K}_3^-\right)_{M\times Nr}, \qquad a^{**} = \left(\mathbf{K}_3^+\right)_{M\times Nr},$$
$$b^* = \left(\mathbf{K}_4^-\right)_{M\times Nr}, \qquad b^{**} = \left(\mathbf{K}_4^+\right)_{M\times Nr},$$
$$c^* = (\mathbf{K}_{51})_{Nr\times M}, \qquad c^{**} = \left(\mathbf{K}_{52}^-\right)_{Nr\times Nr},$$
$$c^{***} = \left(\mathbf{K}_{52}^+\right)_{Nr\times Nr},$$
$$d^* = (\mathbf{K}_{61})_{Nr\times M}, \qquad d^{**} = \left(\mathbf{K}_{62}^-\right)_{Nr\times Nr},$$
$$d^{***} = \left(\mathbf{K}_{62}^+\right)_{Nr\times Nr},$$

and $M$ is the number of nodes. For a given $m$, the azimuthal scattering matrix is defined as:

$$\begin{Bmatrix} \mathbf{P}_{mn}^{I-} \\ \mathbf{P}_{mn}^{II+} \end{Bmatrix} = \mathbf{s}_{2Nr\times 2Nr} \begin{Bmatrix} \mathbf{P}_{mn}^{I+} \\ \mathbf{P}_{mn}^{II-} \end{Bmatrix}. \tag{20}$$

This matrix is obtained by formulating the system of Eq. (23) as follows:

$$\mathbf{Kp} + \mathbf{A}\begin{Bmatrix} \mathbf{P}_{mn}^{I+} \\ \mathbf{P}_{mn}^{II-} \end{Bmatrix} + \mathbf{B}\begin{Bmatrix} \mathbf{P}_{mn}^{I-} \\ \mathbf{P}_{mn}^{II+} \end{Bmatrix} = 0,$$
$$\mathbf{Cp} + \mathbf{U}\begin{Bmatrix} \mathbf{P}_{mn}^{I+} \\ \mathbf{P}_{mn}^{II-} \end{Bmatrix} + \mathbf{V}\begin{Bmatrix} \mathbf{P}_{mn}^{I-} \\ \mathbf{P}_{mn}^{II+} \end{Bmatrix} = 0, \tag{21}$$

where $\mathbf{p}$ is the nodal acoustic pressure vector and the matrices $\mathbf{A}$, $\mathbf{B}$, $\mathbf{C}$, $\mathbf{U}$, and $\mathbf{V}$ are defined as:

$$\mathbf{A} = [\mathbf{K}_3^- \mathbf{K}_4^+], \quad \mathbf{B} = [\mathbf{K}_3^+ \mathbf{K}_4^-], \quad \mathbf{C} = \mathbf{K}_{51} + \mathbf{K}_{61},$$
$$\mathbf{U} = [\mathbf{K}_{52}^- \mathbf{K}_{62}^+], \qquad \mathbf{V} = [\mathbf{K}_{52}^+ \mathbf{K}_{62}^-]. \tag{22}$$

The azimuthal scattering matrix is then written as:

$$\mathbf{s} = \left(\mathbf{V} - \mathbf{C}\mathbf{K}^{-1}\mathbf{B}^{-1}\right)\left(\mathbf{U} - \mathbf{C}\mathbf{K}^{-1}\mathbf{A}^{-1}\right). \tag{23}$$

The total scattering matrix of the studied ducts $\mathbf{S}_{2Nr\times 2Nr}$ is obtained by repeating this operation for each m and by gathering the azimuthal matrices $\mathbf{s}_{2Nr\times 2Nr}$ and $N$ is the total number of modes present in the duct.

## 4. Computation of the acoustic power attenuation

The acoustic power attenuation, $W_{\text{att}}$ of a two ports duct is defined as the ratio between the acoustic powers on both sides of the incoming waves $W^{\text{in}}$ and the outgoing waves $W^{\text{out}}$, as presented by Taktak *et al.* (2010):

$$W_{\text{attenuation}}\ [\text{dB}] = 10\log_{10}\frac{W^{\text{in}}}{W^{\text{out}}} = 10\log_{10}\left(\frac{\sum_{i=1}^{2N}|d_i|^2}{\sum_{i=1}^{2N}\lambda_i|d_i|^2}\right), \tag{24}$$

where $\lambda_i$ are the eigenvalues of the matrix $\mathbf{H}$, defined as:

$$\mathbf{H}_{2N\times 2N} = \left[\mathbf{X}\mathbf{O}_{2N\times 2N}\mathbf{S}_{2N\times 2N}\mathbf{X}\mathbf{I}^{-1}_{2N\times 2N}\right]^{T*}_{2N\times 2N} \cdot\left[\mathbf{X}\mathbf{O}_{2N\times 2N}\mathbf{S}_{2N\times 2N}\mathbf{X}\mathbf{I}^{-1}_{2N\times 2N}\right]_{2N\times 2N}, \tag{25}$$

$$\mathbf{X}\mathbf{I}_{2N\times 2N} = \left[\text{diag}\left(\sqrt{N_{mn}k^{+}_{mn}/2\rho_0 c_0 k}\right)\right]_{2N\times 2N}, \tag{26}$$

$$\mathbf{X}\mathbf{O}_{2N\times 2N} = \left[\text{diag}\left(\sqrt{N_{mn}k^{-}_{mn}/2\rho_0 c_0 k}\right)\right]_{2N\times 2N},$$

$$\{d\}_{2N} = \mathbf{U}^{T*}_{2N\times 2N}\left\{\mathbf{\Pi}^{\text{in}}\right\}_{2N}, \tag{27}$$

where $\mathbf{U}$ is the eigenvectors of the matrix of $\mathbf{H}$ and T* denotes conjugate transpose.

## 5. Description of the used liners

The cylindrical ducts, as used in this study, are treated with two acoustic liners of a locally reactive type. These liners are characterised by their acoustic impedance $Z_a$ and $Z_b$, used as the input for computation of the numerical scattering matrix, as presented in Fig. 2.

The first liner (a: PP-Air cavity) consists of a perforated plate with an air-cavity before the rigid wall. The second liner (b: PP-PM) is composed of a perforated plate backed by an absorbing porous material before the rigid wall. Each of these acoustic liners can provide a different response. To describe the liners' behaviour, two empirical models can be employed. One

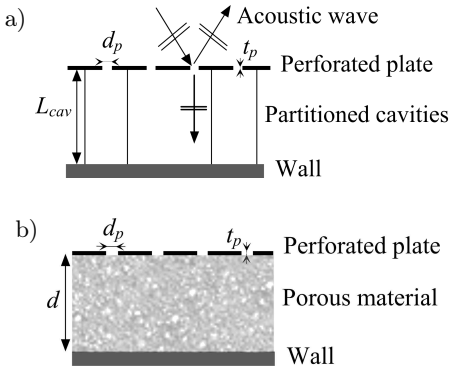


Fig. 2. Composition of the used liner (a) perforated plate + air cavity; (b) perforated plate + porous material.

model, proposed by Elnady (2004), is used to calculate the perforated plate and another model, proposed by Allard (1993) and Lafarge *et al.* (1997), is used to calculate the porous material.

The liner (a) impedance model is expressed as:

$$Z_a = Z_{\text{perforated plate}} + Z_{cav}. \tag{28}$$

The acoustic impedance of the liner (b) can be modelled as follows:

$$Z_b = Z_{\text{perforated plate}} + Z_{\text{porous material}}, \tag{29}$$

with

$$Z_{\text{porous material}} = Z_c\coth\left(jk_c d_m\right). \tag{30}$$

$Z_c$ and $k_c$ are the surface characteristic impedance and propagation constants of the porous material, respectively, and $d_m$ is the material depth. The values of $Z_c$ and $k_c$ are described in the following section, using the Lafarge-Allard model.

### 5.1. Acoustic impedance of the perforated plate

The acoustic impedance of the perforated plate is computed using Elnady model. This model was validated by measurements realised by Elnady and Boden (2003), Elnady *et al.* (2009; 2010) who have shown the accuracy of this model.

The impedance of the perforated plate can be modelled as follows:

$$Z_E = \text{Re}\left\{\frac{ik}{\sigma_p C_D}\left[\frac{t}{F\left(\frac{k'_s d_p}{2}\right)} + \frac{\delta_{re}}{F\left(\frac{k_s d_p}{2}\right)}\right]\right\} + i\,\text{Im}\left\{\frac{ik}{\sigma_p C_D}\left[\frac{t}{F\left(\frac{k'_s d_p}{2}\right)} + \frac{\delta_{im}}{F\left(\frac{k_s d_p}{2}\right)}\right]\right\}, \tag{31}$$

with $C_D$ being the discharge coefficient, $d_p$ being pore diameter, $t$ as plate thickness, $\sigma_p$ being plate porosity, $\delta_{re}$ and $\delta_{im}$ as correction coefficients

$$\delta_{re} = 0.2d_p + 200d_p^2 + 16000d_p^3, \quad \delta_{im} = 0.2856d_p, \tag{32}$$

$$F\left(\frac{k_s d_p}{2}\right) = 1 - \frac{J_1\left(\frac{k_s d_p}{2}\right)}{\frac{k_s d_p}{2} J_0\left(\frac{k_s d_p}{2}\right)},$$
$$F\left(\frac{k'_s d_p}{2}\right) = 1 - \frac{J_1\left(\frac{k'_s d_p}{2}\right)}{\frac{k'_s d_p}{2} J_0\left(\frac{k'_s d_p}{2}\right)}, \tag{33}$$

$k'_s = \sqrt{\frac{-i\omega}{\nu'}}$, $k_s = \sqrt{\frac{-i\omega}{\nu}}$ with $\nu$ as the kinematic viscosity and $\nu' = 2.179\eta/\rho_0$.

### 5.2. Acoustic impedance of the porous material

The acoustic impedance of the porous material is computed by Lafarge-Allard. The accuracy of this model was mentioned by Sagartzazu and Hervella (2008).

The characteristic impedance $Z_c$ and the propagation constant $k_c$ are then expressed as follows:

$$Z_c = \sqrt{\rho K_{LA}}, \qquad k_c = \omega\sqrt{\frac{\rho}{K_{LA}}}, \tag{34}$$

$$\rho = \alpha_\infty \rho_0 \left[1 - j\frac{\sigma\phi}{\rho_0\alpha_\infty\omega}\sqrt{1 + \frac{4j\rho_0\alpha_\infty^2\omega\eta}{\sigma^2\phi^2\Lambda^2}}\right], \tag{35}$$

$$K_{LA} = \gamma P_0 \left[\gamma - \frac{(\gamma - 1)}{1 + \frac{\eta\phi}{j\omega\rho_0 N_{pr} k'_0}\sqrt{1 + \frac{4j\omega\rho_0 N_{pr} k'^2_0}{\eta\phi^2\Lambda'^2}}}\right], \tag{36}$$

where $\alpha_\infty$ and $\phi$ are the material tortuosity and porosity respectively, $\sigma$ is the material flow resistivity, $\rho_0$ is the air density, $\gamma$ is the ratio of specific heats at constant pressures $C_p$ and volumes $C_v$, respectively, defined as follows:

$$\gamma = \frac{C_P}{C_v}. \tag{37}$$

$N_{\mathrm{Pr}}$ is the Prandtl number, $\eta$ is the dynamic viscosity, $\Lambda$ and $\Lambda'$ are the viscous and thermal characteristic lengths, respectively, $P_0$ is the atmospheric pressure, and $k'_0$ is the thermal permeability.

## 6. Numerical results

Six configurations of the lined duct are used to compare two studied liners' acoustic performance on the scattering matrix coefficients and the acoustic power attenuation over the frequency band $ka = [0\ 3.8]$ ($ka$ is the non-dimensional wave number, and $N = 3$ modes are propagating [(0, 0); (1, 0); (2, 0)]). Moreover, the geometries of ducts can change significantly the acoustic liners' behaviour. The porous material is the industrial material "acusticell" as presented in (Sagartzazu, Hervella, 2008), and the used porous characteristics are similar to those used by Othmani *et al.* (2015). Table 1 presents the geometric parameters of each studied configuration. The characteristics of the propagation medium (the air) are listed in Table 2. The different characteristics of the liners (a) and (b) are presented, respectively, in Tables 3 and 4.

Table 1. Geometric parameters of each studied configuration.

| Parameters | $b$ [m] | $c$ [m] | $f$ [m] |
|---|---|---|---|
| Configuration A : straight duct | 0.35 | 0.3 | 0 |
| Configuration $B_1$: sudden narrowing | 0.2 | 0.2 | 0 |
| Configuration $B_2$: progressive narrowing | 0.2 | 0.2 | 0.2 |
| Configuration $C_1$: sudden widening | 0.2 | 0.2 | 0 |
| Configuration $C_2$: progressive widening | 0.2 | 0.2 | 0.2 |

Table 2. The characteristics of the propagation medium (the air).

| Air parameters | |
|---|---|
| Velocity: $c_0$ [m/s] | 340 |
| Density: $\rho_0$ [kg/m$^3$] | 1.2 |
| Characteristic impedance: $Z_0$ [(Pa·s)/m] | 414 |
| Adiabatic constant: $\gamma$ | 1.4 |
| Prandlt Number: $N_{\mathrm{pr}}$ | 0.708 |
| Dynamic viscosity: $\eta$ [Pa·s] | 0.101300 |

Table 3. The different characteristics of the liner (a).

| Liner (a: PP-Air cavity) parameters | |
|---|---|
| Plate thickness: $t$ [m] | 0.001 |
| Pores diameter: $d_p$ [m] | 0.001 |
| Plate porosity: $\sigma_p$ [%] | 2.5 |
| Discharge coefficient: $C_D$ | 0.76 |
| Length of cavity: $L_c$ | 0.02 |

Table 4. The different characteristics of the liner (b).

| Liner (b: PP-PM) parameters | |
|---|---|
| Flow resistivity: $\sigma$ [(N·s)/m] | 22 000 |
| Porosity: $\varphi$ | 0.95 |
| Tortuosity: $\alpha_\infty$ | 1.38 |
| Thermal permeability: $k'_0$ [m$^2$] | $0.83 \cdot 10^{-8}$ |
| Viscous characteristic length: $\Lambda$ [m] | 0.00051 |
| Thermal characteristic length: $\Lambda'$ [m] | 0.024 |
| Thickness of specimen: $d$ [m] | 0.001 |

### 6.1. Configuration A: straight duct

Figure 3 shows the comparison between the effects of the impedance of liners PP-MP and PP-Air cavity of the first configuration A on the acoustic power

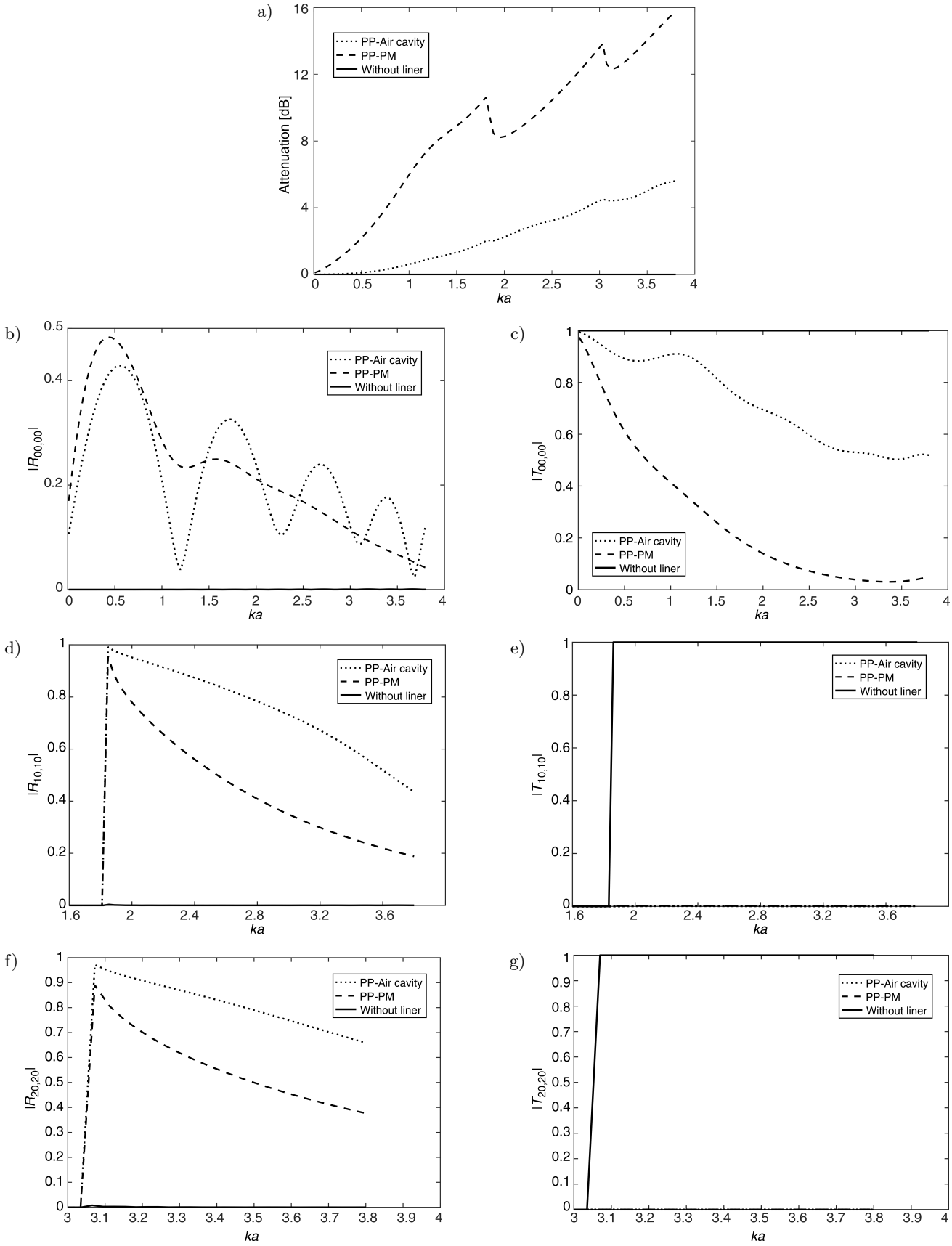


Fig. 3. Comparison of the acoustic behavior (acoustic power attenuation and scattering matrix coefficients in the presence of (0, 0) mode (b, c), (1, 0) mode (d, e), and (2, 0) mode (f, g)) *versus ka* between two acoustic liners' models: PP-PM and PP-Air cavity of configuration A: straight duct.

attenuation and the scattering matrix coefficients, respectively, for the modes (0, 0), (1, 0), and (2, 0) *versus ka*.

Figure 3a reveals that the acoustic power attenuation increases to the final point *versus ka* in the two cases of the studied liners. The attenuation of PP-PM liner yields a good performance in the entire frequency range, however, it shows drops at the mode cut-on frequencies. The maximum attenuation of these liners varies as follows: (PP-Air cavity: 2 dB, $ka$ = 1.8 to 5.5 dB, $ka$ = 3.8; PP-PM: 10.6 dB, $ka$ = 1.8 to 16 dB, $ka$ = 3.8). It was noted that the PP-PM liner is significantly more important, particularly at the high frequency (~5 dB) compared to the PP-Air cavity liner; therefore, it is more efficient. This is explained by the fact that the porous material behind the perforated plate increases the resistance of PP-P liner as mentioned earlier in (Lee *et al.*, 2006), which induces an increase in the attenuation. The modulus of the coefficient $T_{00,00}$ (Fig. 3c) varies conversely from the acoustic power attenuation. $|T_{00,00}|$ decreases from 1 with the increase of $ka$, reaching a minimum of 0.51 for PP-Air cavity and near to zero for PP-PM. This decrease is more remarkable on the PP-PM (~0.5). Figure 3b indicates that the reflection coefficient $R_{00,00}$ increases to a maximum equal to 0.48 in the frequency bands $ka$ = [0–0.5] and then slowly decreases with $ka$ for the PP-PM liner, while a damped oscillation is observed for the PP-Air cavity liner with a maximum amplitude equal to 0.42. The reflection coefficients moduli, $|R_{10,10}|$ and $|R_{20,20}|$ (Figs 3d,f), are close to 1, near the mode cut-on frequencies; then they decrease *versus ka* in the two studied liners cases. Figures 3e,g reveal that the transmissions' coefficients of higher order modes $T_{10,10}$ and $T_{20,20}$ are very close to zero in the two studied liners.

### *6.2. Configuration* $B_1$*: sudden narrowing*

Figure 4 displays the comparison between the effects of the impedance of liner PP-MP and the liner PP-Air cavity of the second configuration $B_1$, having sudden narrowing of a portion duct on the acoustic power attenuation and the scattering matrix coefficients, respectively, for the modes (0, 0), (1, 0), and (2, 0) *versus ka*.

From the figures above it is noticed that the attenuation behaviour of PP-Air cavity liner is similar to that in the configuration A. However, they show a small peak in the frequency band $ka$ = [1.4–2] around the resonance frequency of the liner. The maximum attenuation in this interval passes from 1.9 dB for configuration A to 4 dB for configuration B at $ka$ = 1.77. On the other hand, the attenuation of PP-PM liner decreases significantly, though it does not present drops at the mode cut-on frequencies, compared to that of configuration A. This decrease is intensified with the increase of $ka$. The maximum attenuation varies as follows: (4.9 dB, $ka$ = 1.8; 6.5 dB, $ka$ = 3.05; 6.2 dB, $ka$ = 3.8) for configuration A to (10.6 dB, $ka$ = 1.8; 13.57 dB, $ka$ = 3.05; 15.7 dB, $ka$ = 3.8) for configuration B. It is noted from the figures above that the attenuation behaviour of PP-Air cavity liner is similar to that in the configuration A. However, they shows a small peak in the frequency band $ka$ = [1.4–2] around the resonance frequency of the liner. For the PP-Air cavity liner, the level of attenuation increases and it has negligible drops compared to configuration A. The maximum attenuation passes from 1.9 dB for configuration A to 4 dB for configuration B at $ka$ = 1.77. On the other hand, the level of the attenuation of PP-Air cavity liner decreases significantly with the increase of ka when compared to that of configuration A. The maximum attenuation varies as follows: (4.9 dB, $ka$ = 1.8; 6.5 dB, $ka$ = 3.05; 6.2 dB, $ka$ = 3.8) for configuration A to (10.6 dB, $ka$ = 1.8; 13.57 dB, $ka$ = 3.05; 15.7 dB, $ka$ = 3.8) for configuration B. The moduli of reflection coefficients $R_{00,00}$, $R_{10,00}$ for the two studied liners of this configuration (sudden narrowing) are higher than that of configuration A (straight duct); however, they are slightly lower for $|R_{20,20}|$. The reflection is more important (~0.4 and 0.5) on the (0, 0) mode and (1, 0) mode (~0.4 and 0.5) and less important (~0.4 and 0.5) on the (2, 0) mode, respectively, for the PP-PM liner and the PP-Air cavity liner compared to configuration A. Contrariwise, the moduli of transmission coefficients $T_{00,00}$, $T_{10,00}$, $T_{20,20}$ are weaker. The modulus of the coefficient $R_{00,00}$ indicates that it increases to a maximum (~0.76, $ka$ = 0.4 for PP-PM and ~0.87, $ka$ = 0.6 for PP-Air cavity) and then decreases with $ka$, until reaching 3.7. It is noted that configuration A is more efficient than configuration B in the case of PP-PM liner. Moreover, the attenuation curves, related to the PP-Air cavity liner for the two configurations A and B, are close. This is elucidated by the fact that when the acoustic wave meets the perforated plate, one part of the incident wave is reflected on the perforated plate and another part is reflected on the section discontinuity of the narrowing duct, therefore, resulting in an increase of the reflection. However, the attenuation remains at the same level. To optimise the PP-Air cavity liner, it is interesting to add porous material before the air cavity.

### *6.3. Configuration* $B_2$*: progressive narrowing*

Figure 5 exhibits the comparison between the effects of the impedance of the liner PP-MP and liner PP-Air cavities of configuration $B_2$, having progressive narrowing of a portion duct on the acoustic power attenuation and the scattering matrix coefficients, respectively, for the modes (0, 0), (1, 0), and (2, 0) *versus ka*. These modes reveal that the acoustic behaviour shown in these figures is similar to that of configura-

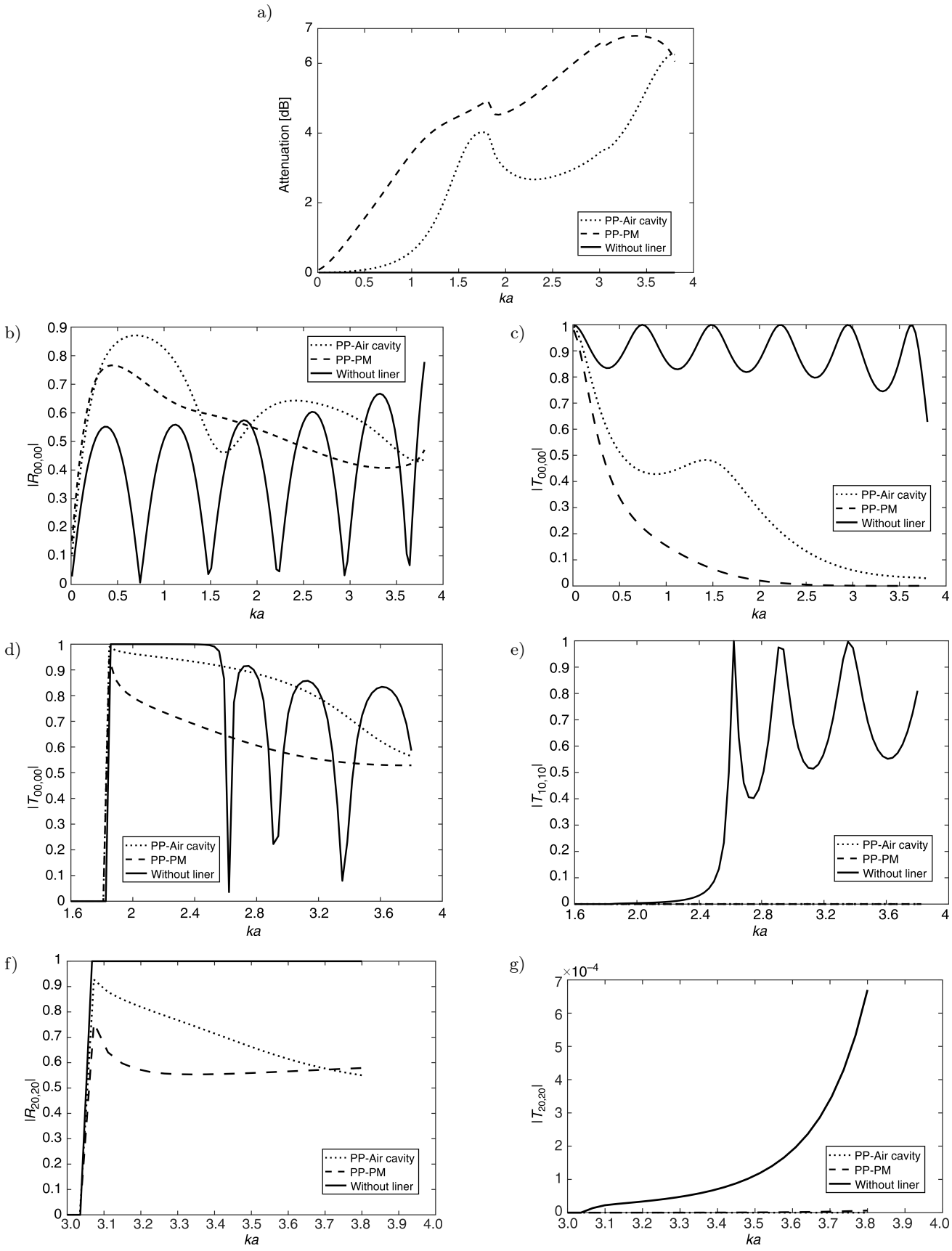


Fig. 4. Comparison of the acoustic behaviour (acoustic power attenuation and scattering matrix coefficients in the presence of (0, 0) mode (b, c), (1,0) mode (d, e), and (2,0) mode (f, g)) *versus ka* between two acoustic liners' models: PP-PM and PP-Air cavity of configuration $B_1$.

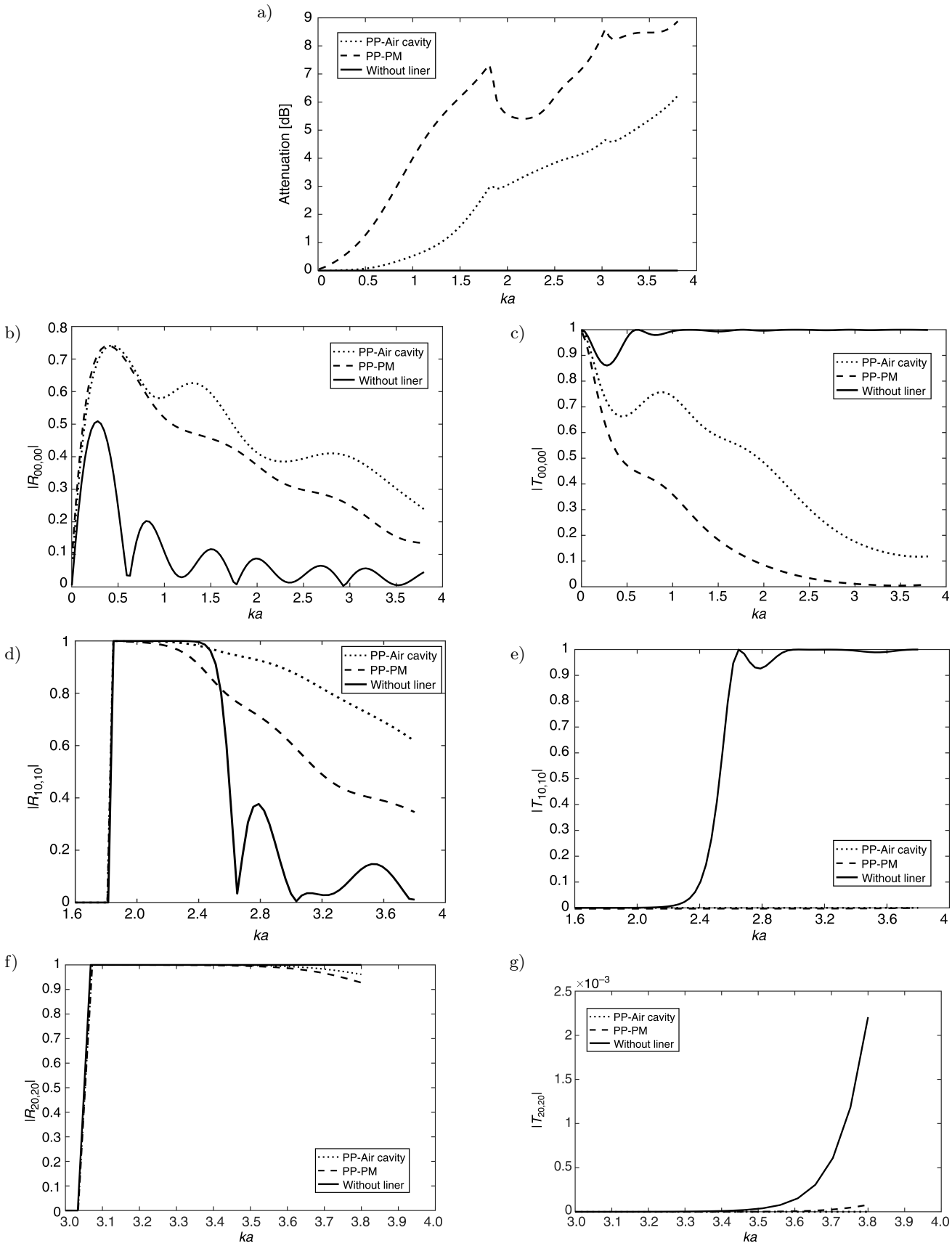


Fig. 5. Comparison of the acoustic behavior (acoustic power attenuation and scattering matrix coefficients in the presence of (0, 0) mode (b, c), (1, 0) mode (d, e), and (2, 0) mode (f, g)) *versus ka* between two acoustic liners' models: PP-PM and PP-Air cavity of configuration $B_2$.

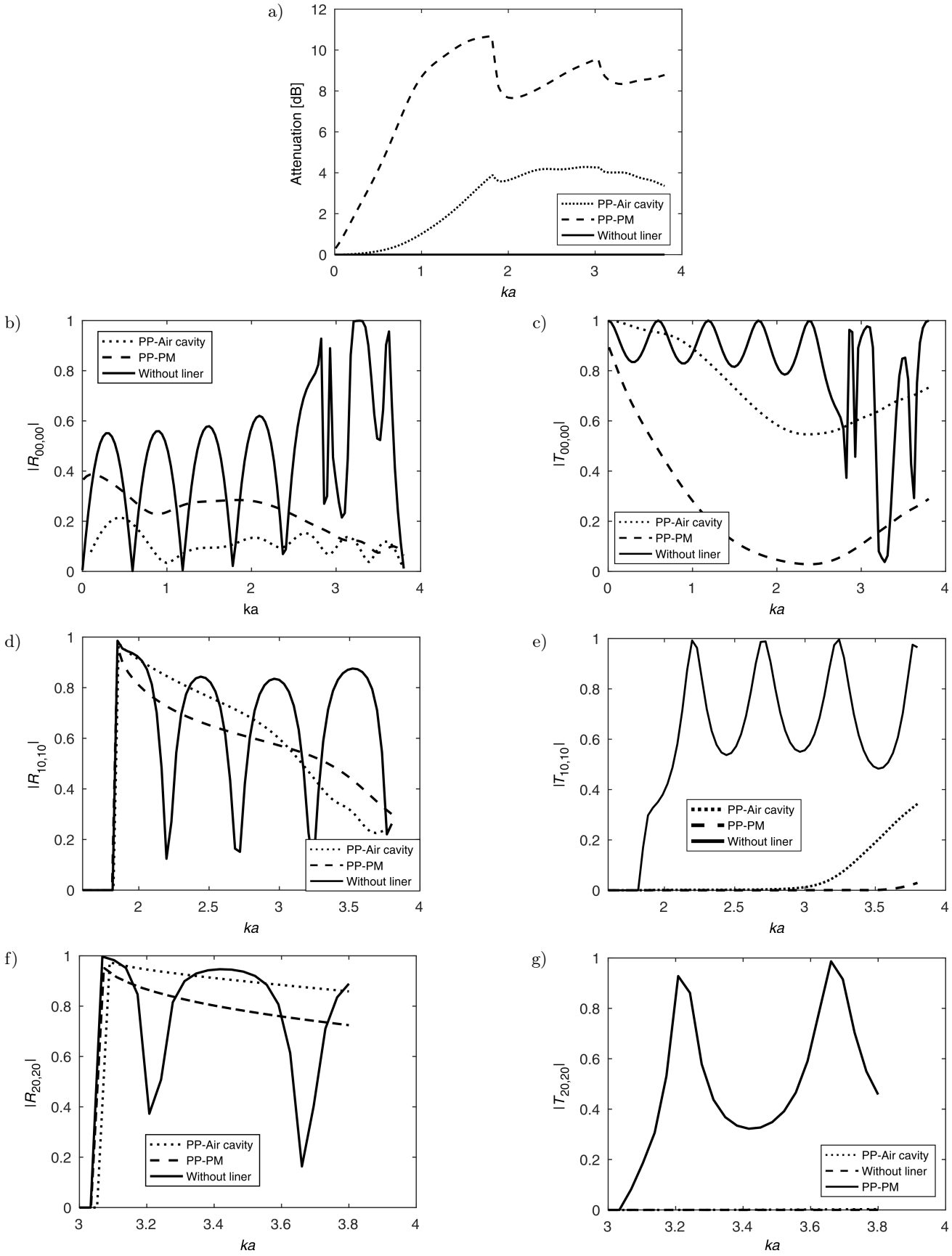


Fig. 6. Comparison of the acoustic behavior (acoustic power attenuation and scattering matrix coefficients in the presence of (0, 0) mode (b, c), (1, 0) mode (d, e), and (2, 0) mode (f, g)) *versus ka* between two acoustic liners' models: PP-PM and PP-Air cavity of configuration $C_1$.

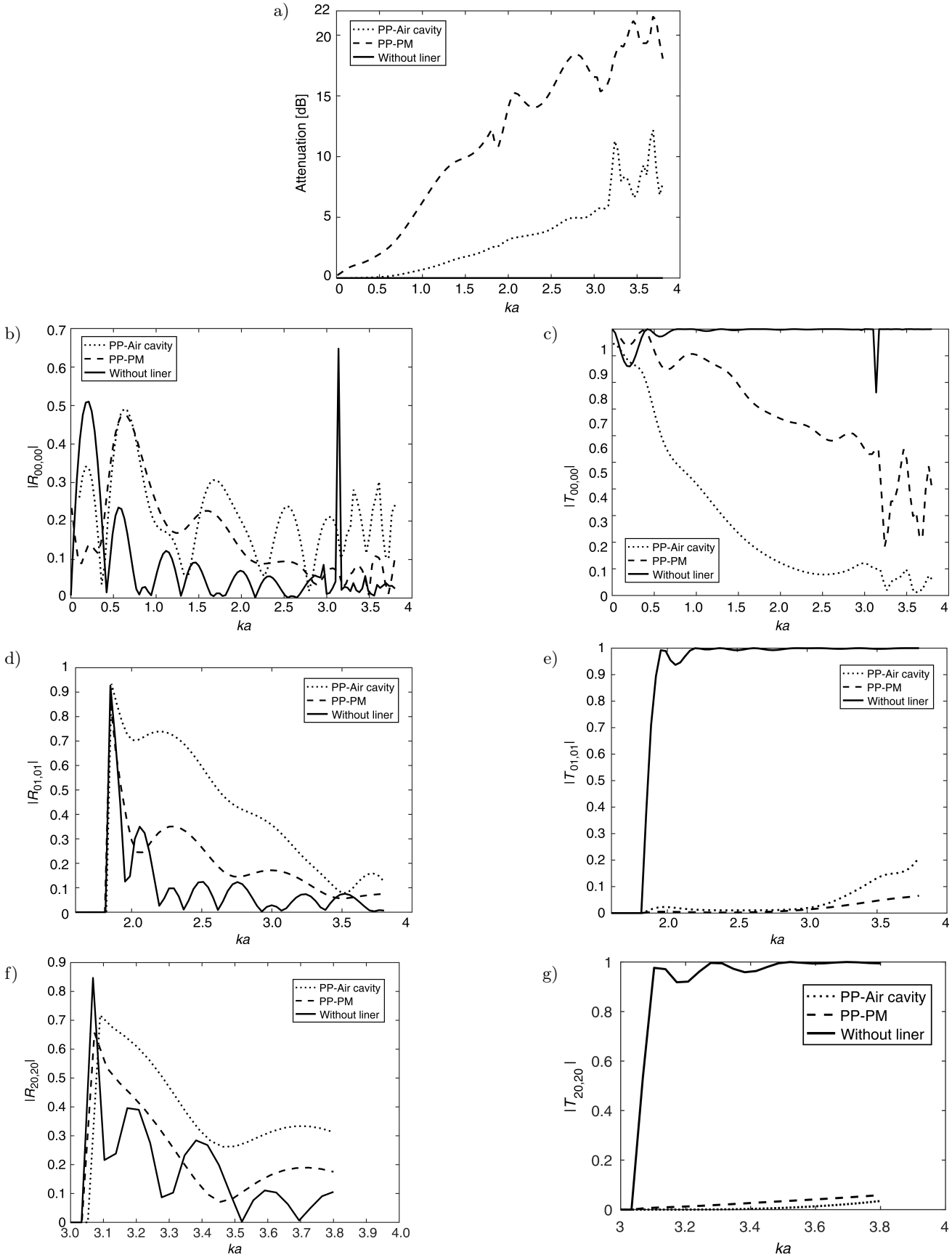


Fig. 7. Comparison of the acoustic behavior (acoustic power attenuation and scattering matrix coefficients in the presence of (0, 0) mode (b, c), (1, 0) mode (d, e) and (2, 0), mode (f, g)) *versus ka* between two acoustic liners' models: PP-PM and PP-Air cavity of configuration $C_2$.

tion $B_1$ (sudden narrowing) with small variations, described as follows: the attenuation curves for the case of the PP-PM liner are identical up to $ka$ = 0.9, where the attenuation of configuration $B_2$ starts to be slightly higher, presenting drops at the mode cut-on frequencies. The attenuation curves for the case of the PP-Air cavity liner are identical up to $ka$ = 0.16, therefore, it is slightly higher in configuration $B_2$, except for that in the frequency range $ka$ = [1.6–2]. The modulus of the coefficient $T_{00,00}$ indicates that it is starting to be slightly higher for $ka$ above 1.2 for the case of PP-PM liner and in $ka \in$ [0.6–2.5] for the case of PP-Air cavity liner compared to configuration $B_1$. Conversely, the modulus of the coefficient $R_{00,00}$ shows that it is slightly lower. However, the reflection coefficients of higher order modes are higher than configuration $B_1$. The (1, 0) mode reflection coefficient reveals that it is equal to 1 at the cut-on frequency and for $ka \in$ [0–2.25] in the case of PP-PM liner, also in $ka \in$ [0–2.24] in the case of PP-Air cavity liner. Then, a small decrease is observed outside these ranges. Hence, configuration $B_2$ filters the modes in this band ("mode conversion" phenomenon from the (1, 0) mode to (2, 0) mode). The (2, 0) mode reflection coefficient is almost totally reflected in both studied liners.

### *6.4. Configuration $C_1$: sudden widening*

Figure 6 represents the comparison between the effects of the impedance of liner PP-MP and the liner PP-Air cavity of the configuration $C_1$, having a sudden widening of the portion duct on the acoustic power attenuation and the scattering matrix coefficients, respectively, for the modes (0, 0), (1, 0), and (2, 0) *versus ka*. By comparing the results of these figures with Fig. 5 for sudden narrowing of the duct, it is noticed that the acoustic power attenuation for both liners is better in the entire frequency range and the maximum attenuation varies as: ($W_{\mathrm{att,max}}$ = 5 dB, $ka$ = 1.8; $W_{\mathrm{att,max}}$ = 6.2 dB, $ka$ = 3.8 for PP-Air cavity liner and $W_{\mathrm{att,max}}$ = 11.2 dB, $ka$ = 1.8; $W_{\mathrm{att,max}}$ = 9 dB, $ka$ = 3.8 for PP-PM liner). The reflection coefficients moduli are lower, except that of the (2, 0) mode, which is slightly higher, and the modulus of transmission coefficient $T_{00,00}$ is higher. We conclude that the duct with a sudden widening portion is more efficient than the duct with a sudden narrowing portion.

### *6.5. Configuration $C_2$: progressive widening*

Figure 7 displays the comparison between the effects of the impedance of liner PP-MP and the liner PP-Air cavity of the configuration $C_2$, having a sudden widening of the portion duct on the acoustic power attenuation and the scattering matrix coefficients, respectively, for the modes (0, 0), (1, 0), and (2, 0) *versus ka*. It can be observed that the acoustical properties of this configuration are significantly affected compared to other studied configurations. The acoustic power attenuation increases when the number $ka$ increases, with small fluctuations observed at $ka$ above 1.8 for the case of PP-PM liner and at $ka$ = 3.2 for the case of PP-Air cavity liner. The maximum attenuation is better in both liners: $W_{\mathrm{att,max}}$ = 12 dB for Air cavity liner and $W_{\mathrm{att,max}}$ = 22 dB for PP-PM liner at $ka$ = 3.6. The modulus of the coefficient $R_{00,00}$ gives close results in both liners and it presents damping unstable, which is more apparent for the PP-PM liner. For both higher-order modes, the scattering matrix coefficients have the same shapes in the two liners' models. The reflection coefficients are less important than configuration $C_1$, inversely, for the transmission coefficients, being a little higher. It is worth noting that this configuration generates evanescent modes at section discontinuity that cause an attenuation perturbation at higher frequencies when coupled with the propagating modes.

## 7. Conclusion

In this paper, a comparison between the influence of two models of acoustic liners was conducted, i.e. PP-MP (a) and PP-Air cavity (b) on the acoustic power attenuation and scattering matrix coefficients on the (0,0), (1,0), (2,0) modes of five configurations of the lined duct were investigated, using the multimodal scattering matrix method. These configurations were described with and without section discontinuities.

It is concluded from the results presented above that:

- the 5th configuration in the case of a progressive widening is the most efficient silencer, especially at high frequencies compared with all the rest of configurations; however, it generates fluctuation of acoustic waves at higher frequencies produced by the evanescent modes;
- the PP-PM liner is more absorbent in the entire frequency range, therefore, being more efficient than the PP-Air cavity liner: the addition of the porous part behind the perforated plate makes it possible to increase the attenuation while decreasing the reflection by acoustic dissipation. It causes an increase in system resistance, which results in an increase in the attenuation.

## Appendix. Attenuation *versus f* for configuration $B_2$ and $C_2$

The values of attenuation for different values of $ka$ when varying $f$ from 0 to 3.5 of configurations $B_2$ and $C_2$, were each treated by liner models PP-Air cavity and PP-PM are listed respectively in Tables 5–8.

Table 5. Values of the attenuation *versus* $f$ for several frequency $ka$ of configuration $B_2$ treated with PP-Air cavity liner model.

| | $f$ [m] | 0 | 0.05 | 0.1 | 0.15 | 0.2 | 0.25 | 0.3 | 0.35 |
|---|---|---|---|---|---|---|---|---|---|
| Attenuation [dB] | $ka$ = 1.8 | 2.34 | 3.1 | 3 | 2.78 | 2.93 | 2.81 | 2.81 | 2.86 |
| | $ka$ = 2.8 | 3.15 | 4.09 | 4.14 | 4.48 | 4.21 | 4.41 | 4.36 | 4.32 |
| | $ka$ = 3.05 | 3.45 | 4.55 | 4.53 | 4.84 | 4.7 | 4.74 | 4.81 | 4.77 |
| | $ka$ = 3.5 | 5.06 | 5.43 | 5.25 | 5.18 | 5.35 | 5.32 | 5.18 | 5.32 |
| | $ka$ = 3.8 | 6.23 | 6.75 | 6.36 | 6.39 | 6.23 | 6.38 | 6.35 | 6.18 |

Table 6. Values of the attenuation *versus* $f$ for several frequency $ka$ of configuration $B_2$ treated with PP-PM liner model.

| | $f$ [m] | 0 | 0.05 | 0.1 | 0.15 | 0.2 | 0.25 | 0.3 | 0.35 |
|---|---|---|---|---|---|---|---|---|---|
| Attenuation [dB] | $ka$ = 1.8 | 5.36 | 5.45 | 8.05 | 8.17 | 7.83 | 8.77 | 8.17 | 8.51 |
| | $ka$ = 2.8 | 5.48 | 6.5 | 7.5 | 8.24 | 7.64 | 8.187 | 8.05 | 8 |
| | $ka$ = 3.05 | 5.67 | 7.45 | 8.95 | 9.4 | 9.091 | 9.55 | 9.43 | 9.56 |
| | $ka$ = 3.5 | 5.6 | 8.1 | 8.5 | 8.4 | 8.6 | 8.6 | 8.4 | 8.6 |
| | $ka$ = 3.8 | 5.055 | 9.2 | 8.62 | 9.14 | 9.96 | 9 | 8.91 | 8.7 |

Table 7. Values of the attenuation *versus* $f$ for several frequency $ka$ of configuration $C_2$ treated with PP-Air cavity liner model.

| | $f$ [m] | 0 | 0.05 | 0.1 | 0.15 | 0.2 | 0.25 | 0.3 | 0.35 |
|---|---|---|---|---|---|---|---|---|---|
| Attenuation [dB] | $ka$ = 1.8 | 2.65 | 2.55 | 2.56 | 2.50 | 2.56 | 2.5 | 2.56 | 2.5 |
| | $ka$ = 2.8 | 3.16 | 5.1 | 5.2 | 4.87 | 4.94 | 4.94 | 4.8 | 4.84 |
| | $ka$ = 3.05 | 3.28 | 5.2 | 6.05 | 5.85 | 5.74 | 5.74 | 5.75 | 5.67 |
| | $ka$ = 3.5 | 2.85 | 6.65 | 9.7 | 8.23 | 7 | 9.46 | 9.6 | 6.6 |
| | $ka$ = 3.8 | 2.45 | 7 | 9 | 13.3 | 7.8 | 14.6 | 9.2 | 14.6 |

Table 8. Values of the attenuation *versus* $f$ for several frequency $ka$ of configuration $C_2$ treated with PP-PM liner model.

| | $f$ [m] | 0 | 0.05 | 0.1 | 0.15 | 0.2 | 0.25 | 0.3 | 0.35 |
|---|---|---|---|---|---|---|---|---|---|
| Attenuation [dB] | $ka$ = 1.8 | 8.4 | 15.36 | 12.71 | 14 | 14 | 13.14 | 13.36 | 13.27 |
| | $ka$ = 2.8 | 9.2 | 19.13 | 19.51 | 17.59 | 17.09 | 18.43 | 17.55 | 18.63 |
| | $ka$ = 3.05 | 9.64 | 18.94 | 20.47 | 17.93 | 17.08 | 17.29 | 17.35 | 16.97 |
| | $ka$ = 3.5 | 8.08 | 18.06 | 18.3 | 19.66 | 19.87 | 19.54 | 20.72 | 18.62 |
| | $ka$ = 3.8 | 7.8 | 16 | 20.4 | 19.7 | 17.95 | 21.7 | 18.86 | 22.2 |

Figure 8 shows the acoustic power attenuation versus $f$ for several $ka$ of configuration $B_2$ treated with PP-Air cavity liner model. These figures show that the attenuation grows slightly for all studied $ka$

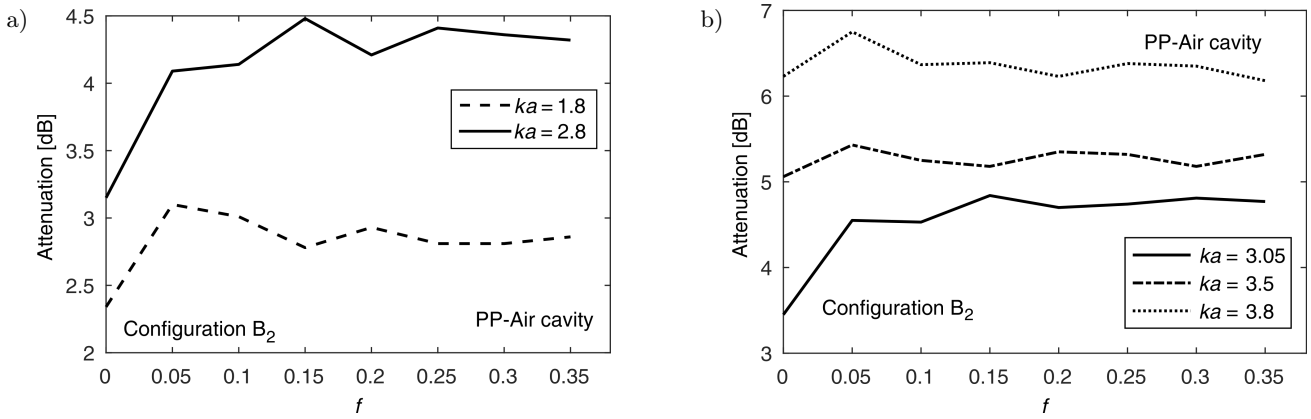


Fig. 8. Acoustic power attenuation versus progressive part $f$ of configuration $B_2$ treated by PP-Air cavity liner model for several $ka$ (a) and (b).

with the presence of the progressive part $f$ and then it presents a small variation when $f$ varies from 0.05 to 0.35.

Figure 9 presents very interesting results which show that if the configuration $B_2$ is treated with PP-PM liner model, the acoustic power attenuation grows strongly with the presence of part $f$ for all studied $ka$ and the acoustic power attenuation varies with and without the progressive part $f$ ($ka$ = 1.8: $W_{\text{att}}$ = 5.36 dB for $f$ = 0 and $W_{\text{att}}$ = 8.05 dB for $f$ = 0.1; $ka$ = 2.8: $W_{\text{att}}$ = 5.48 dB for $f$ = 0 and $W_{\text{att}}$ = 8.24 dB for $f$ = 0.1; $ka$ = 3.05: $W_{\text{att}}$ = 5.67 dB for $f$ = 0 and $W_{\text{att}}$ = 7.45 dB for $f$ = 0.05; $ka$ = 3.5: $W_{\text{att}}$ = 5.6 dB for $f$ = 0 and $W_{\text{att}}$ = 8.1 dB for $f$ = 0.05; $ka$ = 3.8: $W_{\text{att}}$ = 5.05 dB for $f$ = 0 and $W_{\text{att}}$ = 9.2 dB for $f$ = 0.05). A maximum of attenuation is about 8.77 dB for $f$ = 0.25, 8.24 dB for $f$ = 0.15, 9.56 dB for $f$ = 0.35, 8.66 dB for $f$ = 3.5 and 10 dB for $f$ = 2 for $ka$ = 1.8, 2.8, 3.05, 3.5 and 3.8, respectively.

Figure 10 presents the acoustic power attenuation versus $f$ for several $ka$ of configuration $C_2$ treated with the PP-Air cavity liner model. It can be observed from this figure that the attenuation increases with the presence of part $f$ but this increase changes when $f$ varies, except when $ka$ = 1.8, where the attenuation slightly reduces. The results show that the maximum of attenuation according to the frequency is about 5.2 dB, $ka$ = 2.8 for $f$ = 0.05 (3.1 dB for $f$ = 0) and 6 dB, $ka$ = 3.05 for $f$ = 0.1 (3.3 dB for $f$ = 0) and 9.7 dB, $ka$ = 3.5 for $f$ = 0.1 (2.85 dB for $f$ = 0) and 14.6 dB, $ka$ = 3.8 for $f$ = 3.5 (2.45 dB for $f$ = 0).

Figure 11 presents the acoustic power attenuation versus $f$ for several $ka$ of configuration $B_2$ treated with the PP-PM liner model. It shows that the effect of the progressive part $f$ on the attenuation for all studied $ka$ is similar to Fig. 9. The attenuation greatly increased with the presence of part $f$. A maximum of attenuation with and without part $f$ varies: ($ka$ = 1.8: $W_{\text{att}}$ = 8.4 dB for $f$ = 0 and $W_{\text{att,max}}$ = 15.3 dB for $f$ = 0.05; $ka$ = 2.8: $W_{\text{att}}$ = 9.2 dB for $f$ = 0 and $W_{\text{att,max}}$ = 19.5 dB for $f$ = 0.1; $ka$ = 3.05: $W_{\text{att}}$ = 9.6 dB for $f$ = 0 and $W_{\text{att,max}}$ = 20.4 dB for $f$ = 0.1; $ka$ = 3.5: $W_{\text{att}}$ = 8 dB for $f$ = 0 and $W_{\text{att,max}}$ = 20.7 dB for $f$ = 0.3; $ka$ = 7.8: $W_{\text{att}}$ = 9.6 dB for $f$ = 0 and $W_{\text{att,max}}$ = 22.2 dB for $f$ = 0.35. It can be clearly seen that the attenuation is significantly increased if a progressive part for configurations $B_2$ and $C_2$ is introduced.

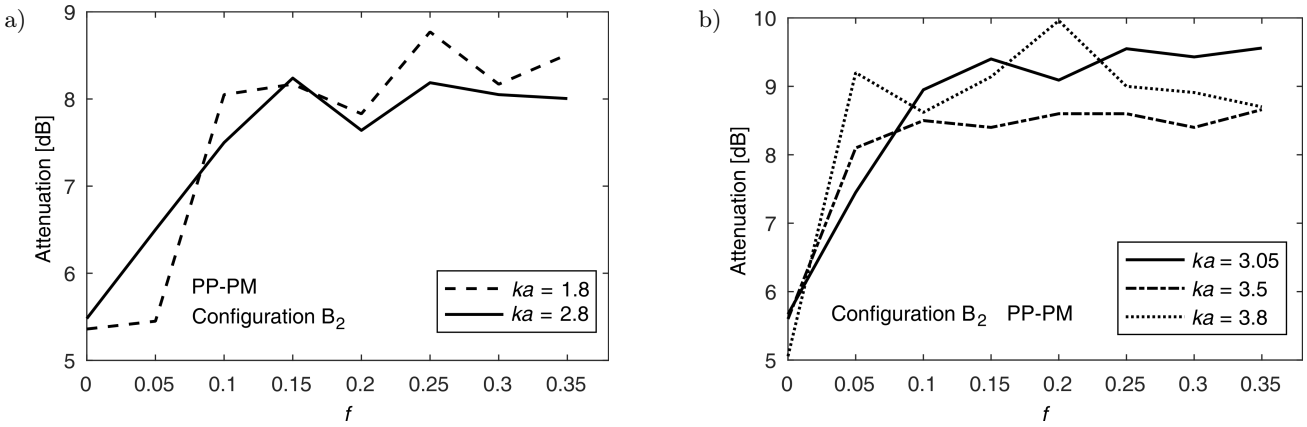


Fig. 9. Acoustic power attenuation versus progressive part $f$ of configuration $B_2$ treated by PP-PM liner model for several $ka$ (a) and (b).

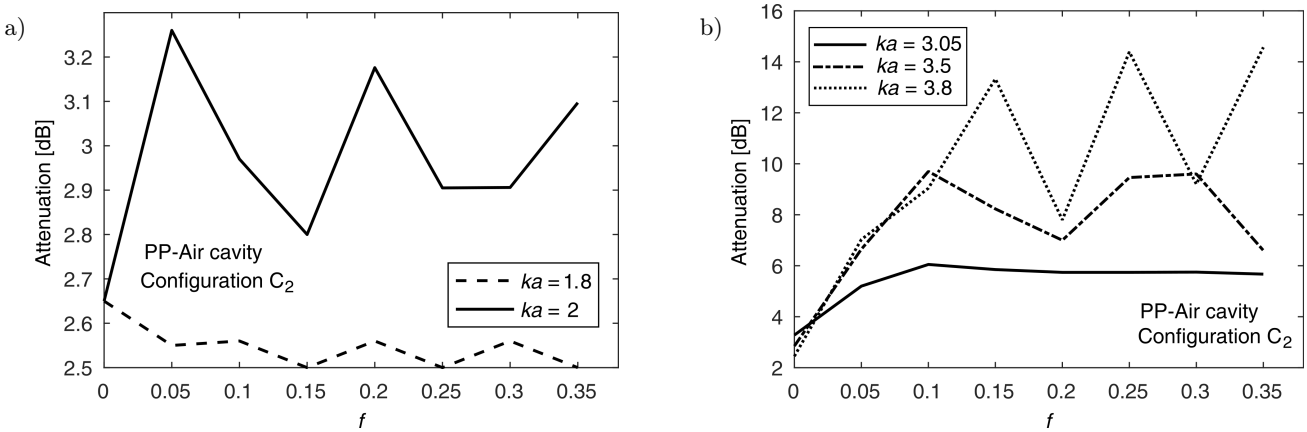


Fig. 10. Acoustic power attenuation versus progressive part f of configuration $C_2$ treated by PP-Air cavity liner model for several $ka$ (a) and (b).

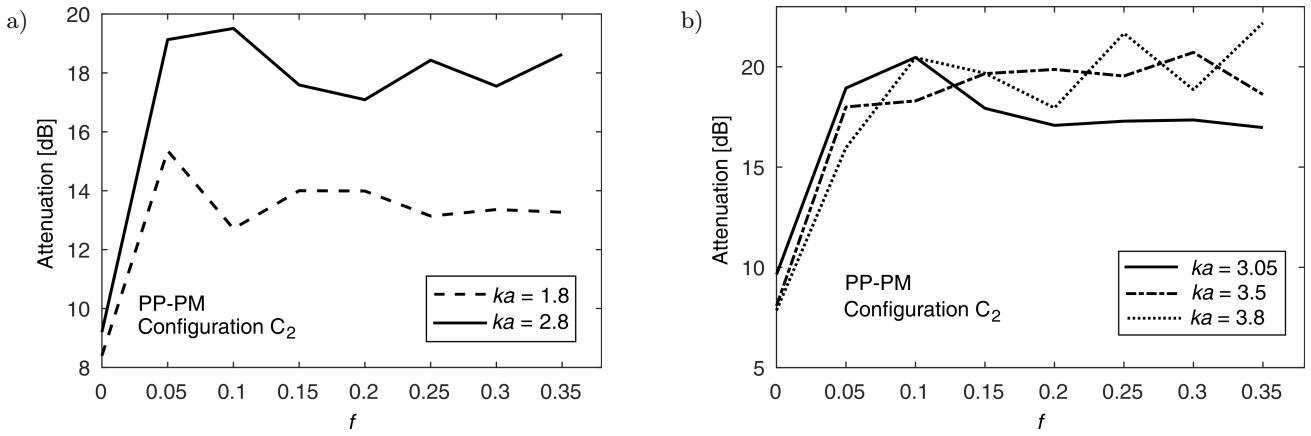


Fig. 11. Acoustic power attenuation versus progressive part f of configuration $C_2$ treated by PP-PM model for several *ka* (a) and (b).

## References

1. Åbom M. (1991), Measurement of the scattering matrix of acoustical two-ports, *Mechanical Systems Signal Processing*, **5**(2): 89–104, doi: 0.1016/0888-3270(91)90017-Y.
2. Allard J.F. (1993), *Propagation of sound in porous media: Modeling sound absorbing materials*, Elsevier Applied Science, London 1993, pp. 105–115.
3. Auger J.M., Ville J.M. (1986), Flow effects on measurement of the modal decomposition of acoustic field in a hard wall cylindrical duct, [in:] Comte-Bellot G., Williams J.E.F. [Eds], *Aero- and Hydro-Acoustics. IUTAM Symposia (International Union of Theoretical and Applied Mechanics*, pp. 437–444, Springer-Verlag, Berlin, Heidelberg, doi: 10.1007/978-3-642-82758-7_41.
4. Aurégan Y., Leroux M., Pagneux V. (2004), Measurement of liner impedance with flow by an inverse method, *10th AIAA/CEAS Aeroacoustics Conference*, Manchester, doi: 10.2514/6.2004-2838.
5. Ben Jdidia M., Akrout A., Taktak M., Hammami L., Haddar M. (2014), Thermal effect on the acoustic behavior of an axisymmetric lined duct, *Applied Acoustics*, **86**: 138–145, 10.1016/j.apacoust.2014.03.004.
6. Bodén H., Kabral R. (2015), The effect of high temperatures and grazing flow on the acoustic properties of liners, *Proceedings of Euronoise 2015*, C. Glorieux [Ed.], Maastricht, June 1–3, 2015, pp. 2261–2266.
7. Busse-Gerstengarbe S. *et al.* (2012), Impedance eduction based on microphone measurements of liners under grazing flow conditions, *AIAA Journal*, **50**(4): 867–879, doi: 10.2514/1.J051232.
8. Busse-Gerstengarbe S., Bake F., Enghardt L., Jones M.G. (2013), Comparative study of impedance eduction methods, Part 1: NASA tests and methodologies, *AIAA-2124, 19th AIAA/CEAS Aeroacoustics Conference*, Berlin, Germany, doi: 10.2514/6.2013-2124.
9. Demir A. (2016), Sound transmission in a duct with sudden area expansion, extended inlet and lined walls in overlapping region, *Advances in Acoustic and Vibration*, **2016**, Article ID 9485163, 8 pages, doi: 10.1155/2016/9485163.
10. Demir A. (2017), Scattering matrices in non-uniformly lined ducts, *Zeitschrift für angewandte Mathematik und Physik*, **68**(1): 8, doi: 10.1007/s00033-016-0754-8.
11. Dhatt G., Touzot G. (1989), *Presentation of the finite element method*, Maloine S.A. Editeur, Paris.
12. El-Masri S. (2004), Analysis of discontinuities in rectangular ducts and higher order mode excitations using TLM and FEM methods, *Journal of Numerical Modelling, Electronic Networks, Devices and Fields*, **17**: 353–364, doi: 10.1002/jnm.532.
13. Elnady T. (2004), *Modelling and characterization of perforates in lined ducts and mufflers*, Ph.D. Thesis, The Royal Institute of Technology (KTH), Stockholm, Sweden.
14. Elnady T., Åbom M., Allam S. (2010), Modeling perforated tubes in mufflers using two-ports, *ASME Journal of Vibration and Acoustics*, **132**(6): 061010, doi: 10.1115/1.4001510.
15. Elnady T., Boden H. (2003), On semi-empirical liner impedance modeling with grazing flow, *Proceedings of 9th AIAA/CEAS Aeroacoustics Conference and Exhibit*, pp. 1815–1825, May 12–14, 2003, Hilton Head, South Carolina, doi: 10.2514/6.2003-3304.
16. Elnady T., Elsaadany S., Åbom M. (2009), Investigation into Modeling of Multi-Perforated, Mufflers, *16th International Congress on Sound and Vibration*, Krakow, Poland, July 6–9.
17. Jones M.G., Watson W.R. (2011), On the use of experimental methods to improve confidence in educed impedance, *17th AIAA/CEAS Aeroacoustics Conference (32nd AIAA Aeroacoustics Conference)*, No. AIAA 2011-2865, Portland, Oregon, doi: 10.2514/6.2011-2865.
18. Jones M.G., Watson W.R., Howerton B.M., Busse-Gerstengarbe S. (2013), Comparative study

of impedance eduction methods, Part 2: DLR tests and methodologies, *19th AIAA/CEAS Aeroacoustics Conference*, AIAA-2125, Berlin Germany, doi: 10.2514/6.2013-2125.

19. Kabral R., Bodén H., Elnady T. (2014), Determination of liner impedance under high temperature and grazing flow conditions, *20th AIAA/CEAS Aeroacoustics Conference*, AIAA-2956, Atlanta, GA, USA, doi: 10.2514/6.2014-2956.
20. Lafarge D., Lemarinier P., Allard J.F., Tarnow V. (1997), Dynamic compressibility of air in porous structures at audible frequencies, *Journal of Acoustical Society of America*, **102**(4): 1995–2006, doi: 10.1121/1.419690.
21. Lee I.L., Selamet A., Huff N.T. (2006), Acoustic impedance of perforations in contact with fibrous material, *Journal of Acoustical Society of America*, **119**(5): 2785–2797, doi: 10.1121/1.2188354.
22. Masmoudi A., Makni A., Taktak M., Haddar M. (2017), Effect of geometry and impedance variation on the acoustic performance of a porous material lined duct, *Journal of Theoretical and Applied Mechanics*, **55**(2): 679–694, doi: 10.15632/jtam-pl.55.2.679.
23. Miles J. (1946a), The analysis of plane discontinuity in cylindrical tubes, Part I, *Journal of the Acoustical Society of America*, **17**(3): 259–271, doi: 10.1121/1.1916327.
24. Miles J. (1946b), The analysis of plane discontinuity in cylindrical tubes, Part II, *Journal of the Acoustical Society of America*, **17**(3): 272–284, doi: 10.1121/1.1916328.
25. Muehleisen R.T. (1996), *Reflection, radiation, and coupling of higher order modes at discontinuities in finite length rigid walled rectangular ducts*, Ph.D. Thesis, Pennsylvania State University, USA.
26. Othmani C., Hentati T., Taktak M., Elnady T., Fakhfakh T., Haddar M. (2015), Effect of liner characteristics on the performance of duct systems, *Archives of Acoustics*, **40**(1): 117–127, doi: 10.1515/aoa-2015-0014.
27. Sagartzazu X., Hervella-Nieto L., Pagalday J.M. (2008), Review in sound absorbing materials, *Archives of Computational Methods in Engineering*, **15**(3): 311–342, doi: 10.1007/s11831-008-9022-1.
28. Sitel A., Ville J.M., Foucart F. (2003), An experimental facility for measurement of acoustic transmission matrix and acoustic power dissipation of duct discontinuity in higher order modes propagation conditions, *Acta Acustica United with Acustica*, **89**: 586–594.
29. Sitel A., Ville J.M., Foucart F. (2006), Multiload procedure to measure the acoustic scattering matrix of a duct discontinuity for higher order mode propagation conditions, *Journal of the Acoustical Society of America*, **120**(5): 2478–2490, doi: 10.1121/1.2354040.
30. Taktak M., Majdoub M., Ben Tahar M., Haddar M. (2013), Numerical characterization of an axisymmetric lined duct with flow using multimodal scattering matrix, *Journal of Theoretical and Applied Mechanics*, **51**(2): 313–325.
31. Taktak M., Majdoub M.A., Ben Tahar M., Haddar M. (2012), Numerical modelling of the sound propagation in axisymmetric lined flow duct, *Archives of Acoustics*, **37**(1): 151–160.
32. Taktak M., Ville J.M., Haddar M., Foucart F. (2008), Evaluation of a lined duct performance based on a 3D two ports scattering matrix, *Proceedings of Meetings in Acoustics*, **4**(1), doi: 10.1121/1.2975221.
33. Taktak M., Ville J.M., Haddar M., Gabard G., Foucart F. (2010), An indirect method for the characterization of locally reacting liners, *Journal of the Acoustical Society of America*, **127**(6): 3548–3559, doi: 10.1121/1.3365250.
34. Ville J.M. (2014), Experimental methods in duct acoustics for higher order modes propagation conditions, *Proceedings of Forum Acousticum*, Krakow.
35. Watson W.R., Jones M.G. (2013), A Comparative study of four impedance eduction methodologies using several test liners, *19th AIAA/CEAS Aeroacoustics Conference*, AIAA-2274, Berlin, Germany, doi: 10.2514/6.2013-2274.